第32卷第10期 焊 接 学 报 Vol. 32 No. 10
2011年10月 TRANSACTIONS OF THE CHINA WELDING INSTITUTION October 2011

TIG 填锌丝对接焊接镁铝异种金属

刘 飞， 张兆栋， 刘黎明
(大连理工大学 辽宁省先进连接技术重点实验室，大连 116024)

刘 飞

摘 要： 采用普通 TIG 电弧作为焊接热源，对镁铝异种金属进行填加锌丝的对接焊试验. 并利用金相显微镜、电子探针(EPMA)、万能力学性能拉伸机等现代分析手段对所得到的接头进行测试分析. 结果表明，采用这种工艺得到了锌基的合金化焊缝，实现了6061 铝合金和 AZ31B 镁合金的连接，焊缝主要由 $MgZn_2$ 和少量的铝、锌的固溶体构成，焊缝和铝合金母材之间不存在明显的过渡层，和镁合金母材之间有厚约 20～100 μm 的过渡层. 焊缝的硬度高于 6061 铝合金和 AZ31B 镁合金母材. 对接接头的抗拉强度达到 75 MPa.

关键词： 镁铝异种金属；填锌丝对接焊；微观组织；力学性能；TIG
中图分类号： TG401 **文献标识码：** A **文章编号：** 0253－360X(2011)10－0049－04

0 序 言

由于镁合金比强度高、电磁屏蔽性好、易回收，铝合金力学性能高、抗腐蚀性好，因此镁合金和铝合金被广泛应用在航空航天、汽车交通、电子仪表等行业中[1]. 实现镁合金和铝合金的焊接能发挥两种金属不同的使用性能. 因此采用合理的焊接工艺对镁铝异种金属进行焊接研究，具有重要的理论意义和实际应用价值.

目前已有很多学者对镁铝异种金属的焊接性进行了研究. 结果表明，镁铝异种金属采用热熔焊时，Al 元素向镁母材中的扩散较少，而 Mg 元素易向铝母材中扩散形成扩散层，扩散到铝母材中的 Mg 元素与铝形成 $Mg_{17}Al_{12}$，Al_3Mg_2 等金属间化合物，致使扩散层成为接头的力学性能薄弱区[2]. 镁铝异种金属采用爆炸焊时，被焊材料结合面表面呈波浪形，结合面有约 3.5 μm 扩散层，其间夹有规则的熔融后凝固的颗粒，所得到的接头抗剪强度为 70 MPa[3].

镁铝异种金属采用搅拌摩擦焊搭接焊时，搭接材料的上下板过渡区中包含有 $Al_{12}Mg_{17}$，Al_3Mg_2 和 Mg_2Si 等金属间化合物. 当采用较低的焊接速度时，接头中不产生宏观裂纹，强度比采用高速焊接时有所提高[4]. 镁铝异种金属采用激光中间搭接焊时，熔池的底部有一层金属间化合物层，当改用边缘搭接焊时，金属间化合物层减薄，接头的抗拉强度提高[5]. 从目前的报道可知，无论是传统的 TIG 焊、扩散焊还是新兴的激光焊、搅拌摩擦焊，焊接接头中都有金属间化合物生成，这些金属间化合物严重降低接头的力学性能. 文中采用在焊接时填加锌丝，形成以锌为主要成分的合金化焊缝，避免镁铝的直接接触从而减少镁铝金属间化合物的生成，提高了接头的力学性能，为探索出更适合焊接镁铝的焊接工艺奠定基础.

收稿日期：2010－08－31
基金项目：中央高校基本科研业务费资助项目(DUT10ZD108)；辽宁省博士启动基金资助项目(20091010)

1 试验方法

试验材料为直径 3 mm 的锌丝，6061 铝合金和 AZ31B 变形镁合金板材，其化学成分见表 1. 板材的尺寸为 100 mm×50 mm×1.7 mm.

试验前用砂纸去除镁板、铝板以及锌丝表面的氧化层，用丙酮清洗掉板材和锌丝表面的油污. 板材开 120°V 形坡口，对接形式见图 1. 焊接工艺参数为交流标准 TIG 焊，焊枪与水平面倾斜角度约 45°，电流 80 A，焊接速度 400 mm/min，普通氩气保护，流量 16 L/min，填丝速度约 400 mm/min.

焊后用线切割垂直于焊缝切取试样进行力学性能测试. 接头腐蚀后用金相显微镜观察接头的组织，腐蚀液采用的是 5 g 苦味酸＋10 mL 醋酸＋10 mL 水＋100 mL 酒精. 用 EPMA 的定量分析结合二次电子图像来分析焊缝中 Mg，Al 和 Zn 元素的分布

表1 试验材料的化学成分(质量分数,%)

Table 1 Chemical composition of these experimental materials

	Al	Mg	Zn	Si	Cu	Fe	Mn
6061铝合金	余量	0.80~1.20	0~0.25	0.40~0.80	0.15~0.40	0~0.70	0~0.15
AZ31B镁合金	2.50~3.50	余量	0.50~1.50	0.10	0.05	0.005	0.20~0.50
锌丝	0~0.30	—	余量	0~0.03	—	0~0.04	—

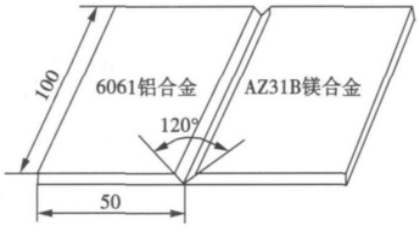

图1 试件尺寸及接头示意图(mm)

Fig. 1 Specimen size and schematic diagram of welding joint

位置和状态,定量分析所用电子束直径为1 μm.

2 试验结果和讨论

2.1 焊缝的表面形貌和接头的宏观形貌

焊缝的正面、背面形貌和接头的宏观形貌如图2所示. 由图2a焊缝的正面和背面成形可以看出焊缝表面成形连续,无明显的咬边. 但焊缝正面有少量的凹陷,这是由于锌的熔沸点较低,焊接时锌的蒸发损失严重造成的. 图2b是焊接接头的宏观形貌,可以看出焊缝中存在着零散分布的气孔,是焊接过程中锌蒸气没逸出焊缝所致. 由于镁和铝的电导率不同,焊接时电弧向铝合金一侧微偏,铝合金一侧的锌丝蒸发损失更严重,导致铝合金侧的焊缝余高低于镁合金.

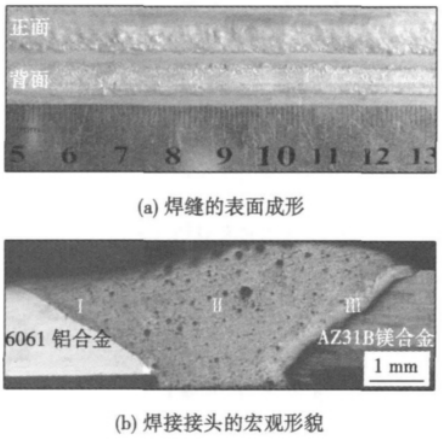

(a) 焊缝的表面成形

(b) 焊接接头的宏观形貌

图2 焊缝的表面成形和焊接接头的宏观形貌

Fig. 2 Surface and cross-section appearance of weld seam

2.2 镁铝异种金属填锌对接焊接头微观组织特征

2.2.1 铝合金母材侧焊缝的微观组织特征

对图2b所示接头宏观形貌的铝母材侧、焊缝中心、镁母材侧分别进行放大来观察其微观组织特征. 图3a为铝母材侧焊缝(图2b中Ⅰ所示位置)的金相组织形貌. 从图3a中可以看出,铝合金母材和焊缝没有明显的过渡层. 靠近铝合金母材部位的焊缝散热较快,晶粒比较细小,约为10~15 μm;远离铝合金母材的焊缝晶粒有所长大,约为15~20 μm. 图3b为与图3a相同部位的二次电子图像,图3b中标注点1处为枝晶间析出物,标注点2处为枝晶,其成分见表2. 枝晶间的析出物主要含有Al和Zn两种元素,结合Al-Zn二元相图,枝晶间析出物为α-Al和β-Zn的复杂混合物. 标注点2处的相根据其成分分析应该是$MgZn_2$.

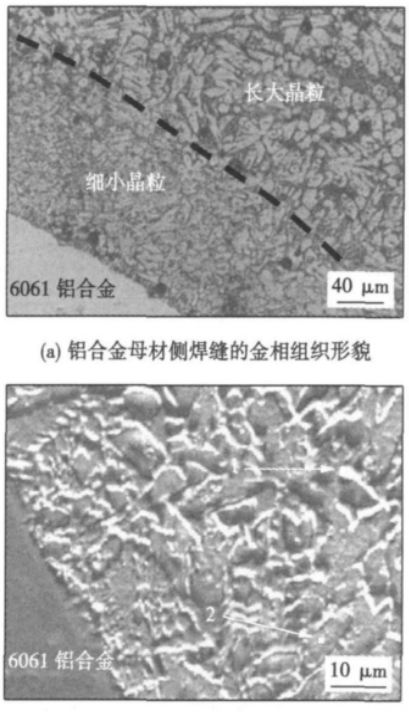

(a) 铝合金母材侧焊缝的金相组织形貌

(b) 铝合金母材侧焊缝的EPMA二次电子像

图3 铝合金母材侧的金相形貌和EPMA二次电子像

Fig. 3 Weld metallographic morphology and EPMA secondary electron image near 6061

表 2　二次电子图像中标注点成分(摩尔分数,%)

Table 2　Components of annotation points in secondary electron image

	Mg	Al	Zn	相组成
1	1.14	26.51	72.34	α-Al,β-Zn
2	30.01	2.02	67.97	$MgZn_2$
3	7.65	18.15	74.20	α-Al,β-Zn,少量 $MgZn_2$
4	30.42	0.93	68.64	$MgZn_2$
5	49.18	0.93	47.18	MgZn
6	53.16	3.42	43.42	γ-Mg,少量 MgZn

2.2.2　焊缝中心的微观组织特征

图 4a 为焊缝中心(图 2b 中Ⅱ所示位置)的金相组织形貌,从图 4a 中可以看出焊缝中心主要有枝状晶组成,存在少量的气孔和夹渣. 对比铝合金母材附近的焊缝,焊缝中心含有的晶间析出物比较少; 焊缝中心枝晶约为 30 ~ 40 μm,比铝合金母材附近的枝晶尺寸大,这是由于焊缝中心冷却较慢,晶粒容易长大. 图 4b 为焊缝中心的二次电子图像,图 4b 中标注点 3 处为枝晶间析出物,其成分和铝合金母材附近的枝晶间析出物成分不同,镁、铝含量增多,结合 Al-Zn-Mg 三元相图推测,此析出物是铝基固溶体(α-Al)及锌基固溶体(β-Zn)以及少量的 $MgZn_2$. 标注点 4 处枝晶成分与铝侧附近的枝晶成分接近,为 $MgZn_2$.

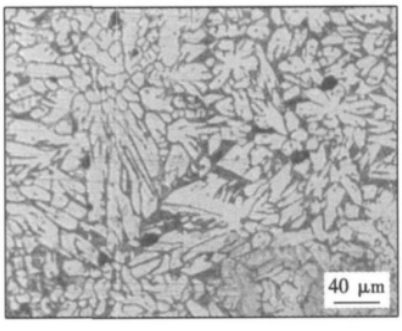

(a) 焊缝中心的金相组织形貌

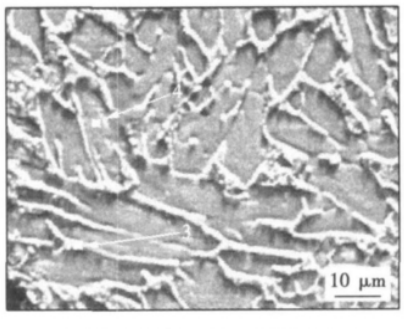

(b) 焊缝中心的EPMA二次电子图像

图 4　焊缝中心的金相组织形貌和 EPMA 二次电子图像

Fig. 4　Weld metallographic morphology and EPMA secondary electron image in center of weld

2.2.3　镁合金母材侧焊缝的微观组织特征

图 5a 为镁合金母材侧焊缝(图 2b 中Ⅲ所示位置)的金相组织形貌. 焊缝和镁合金母材之间存在着厚约为 20 ~ 100 μm 的过渡层. 从图 5a 中可以看出从焊缝中心到镁合金母材依次为: a 树枝晶,b 胞状晶,c 过渡层,d 镁合金母材. 其中树枝晶和胞状晶的成分接近相同,这种结晶状态的差异是由凝固时的过冷度不同造成的[6].

图 5b 为图 5a 中 c 区局部的 EPMA 二次电子图像,标注点 5 处的颗粒主要含有 Mg,Zn 两种元素,其摩尔分数比接近 1∶1,为 MgZn 化合物,过渡层中零散分布着这种化合物颗粒. 标注点 6 处的过渡层 Mg 元素含量升高,根据相图推测由镁的固溶体(γ-Mg)和 MgZn 化合物构成. 从图 5a 中可以看出焊缝从上部到底部过渡层逐渐变窄,这是由于焊接时焊缝上部的金属高温区存在的时间比焊缝底部长,焊缝上部 Mg 原子扩散的时间较长造成的.

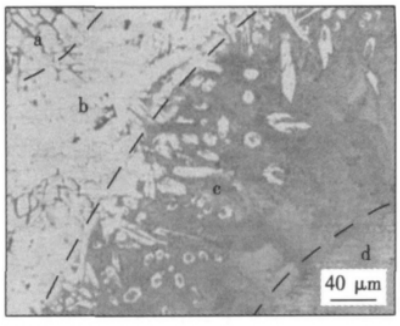

(a) 镁合金母材侧焊缝的金相组织形貌

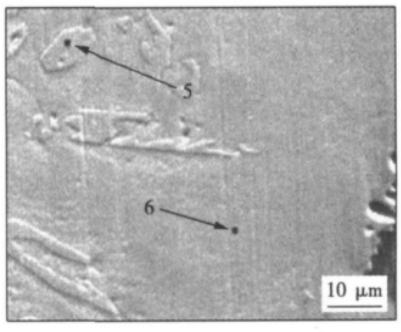

(b) 镁合金母材侧焊缝的EPMA二次电子图像

图 5　镁合金母材侧焊缝的金相组织形貌和 EPMA 二次电子图像

Fig. 5　Weld metallographic morphology and EPMA secondary electron image near AZ31B

由以上分析表明,焊缝主要由 $MgZn_2$ 和少量的铝、锌、镁的固溶体构成. 对比镁铝直接对接焊,没有大量镁铝金属间化合物的生成. 由于镁铝金属间化合物会显著降低接头的力学性能[7],此方法通过

引入Zn元素,形成了锌基的合金化焊缝,避免了镁铝金属间化合物的生成.

2.3 接头显微硬度和力学性能

对镁铝异种金属填锌焊对接接头的镁合金母材、焊缝和铝合金母材进行显微硬度测试,其硬度分布见图6. 测试采用HVS-1000维氏硬度计,载荷为0.98 N,加载时间为15 s. 焊缝显微硬度明显高于两侧母材的显微硬度. 铝合金母材侧的焊缝硬度比镁合金母材侧的焊缝硬度低. 6061铝合金和AZ31B镁合金母材的硬度差别不大,为50~80 HV,镁合金母材侧的焊缝硬度最高达到374.6 HV.

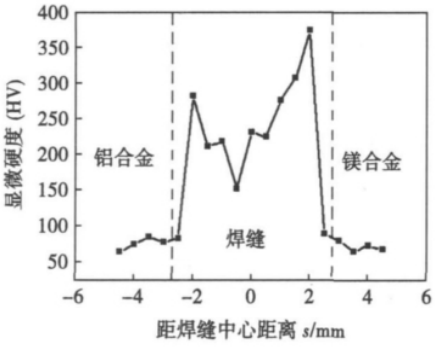

图6 镁铝异种金属填锌焊接头的显微硬度分布

Fig. 6 Microhardness distribution of welded joint

对所得到接头进行抗拉强度测试,强度为75 MPa,远远高于镁铝直接采用热熔焊对接接头的强度[2]. 试样的拉伸接头断裂位置如图7所示,都靠近镁合金母材一侧.

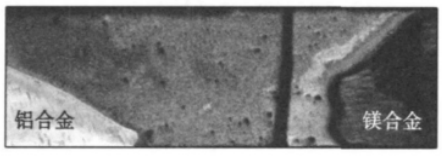

图7 焊接接头的断裂位置

Fig. 7 Fracture locations of joints

3 结 论

(1) 通过填入锌丝实现了6061铝合金和AZ31B镁合金的连接,所得焊缝表面成形连续,接头抗拉强度达到75 MPa.

(2) 焊缝主要由$MgZn_2$和少量的铝、锌、镁的固溶体组成,没有大量的镁铝金属间化合物生成,焊缝与铝合金母材之间不存在明显的过渡层,与镁合金母材之间有厚约为20~100 μm的过渡层.

(3) 焊缝的硬度明显高于6061铝合金和AZ31B镁合金母材,且铝合金母材侧焊缝的硬度比镁合金母材侧焊缝的硬度低,断裂都发生在靠近镁合金母材的一侧.

参考文献:

[1] 曾荣昌, 柯 伟, 徐永波, 等. 镁合金的最新发展及应用前景[J]. 金属学报, 2001, 37(7): 673-685.
Zeng Rongchang, Ke Wei, Xu Yongbo, *et al*. The latest developments and prospects of magnesium alloy [J]. Metallurgica Sinica, 2001, 37(7): 673-685.

[2] 王 恒, 刘黎明, 柳绪静. 镁铝异种材料TIG焊接接头扩散行为分析[J]. 焊接学报, 2005, 26(7): 5-8.
Wang Heng, Liu Liming, Liu Xujing. Diffusion behavior analysis of TIG welded joint between dissimilar materials Mg and Al [J]. Transactions of the China Welding Institution, 2005, 26(7): 5-8.

[3] Yan Y B, Zhang Z W, Shen W, *et al*. Microstructure and properties of magnesium AZ31B-aluminum 7075 explosively welded composite plate [J]. Materials Science and Engineering A, 2010, 527(9): 2241-2245.

[4] Chen Y C, Nakata K. Friction stir lap joining aluminum and magnesium alloys [J]. Scripta Materialia, 2008, 58(6): 433-436.

[5] Rattana Borrisutthekul, Yukio Miyashita, Yoshiharu Mutoh. Dissimilar material laser welding between magnesium alloy AZ31B and aluminum alloy A5052-O [J]. Science and Technology of Advanced Materials, 2005, 6(2): 199-204.

[6] 黄积荣. 铸造合金金相图谱[M]. 北京: 机械工业出版社, 1985.

[7] Zhao L M, Zhang Z D. Effect of Zn alloy interlayer on interface microstructure and strength of diffusion-bonded Mg-Al joints [J]. Scripta Materialia, 2008, 58(4): 283-286.

作者简介: 刘 飞,男,1986年出生,硕士研究生. 主要从事镁铝异种金属焊接技术研究. 发表论文1篇. Email: liufei33733@163.com

通讯作者: 张兆栋,男,讲师. Email: skyezzd@dlut.edu.cn

stress

Effect of welding sequences on welding residual stress and distortion of T-joint LI Chaowen, WANG Yong, HAN Tao (College of Mechanical and Electronic Engineering, China University of Petroleum, Dongying 257061, China). p 37 - 40

Abstract: This paper analyzes the thermo mechanical behavior and evaluates the welding residual stresses and distortion with various types of welding sequence in T-joint welds by performing thermal elasto-plastic analysis using finite element techniques. The 3-D solid elements are used in FE model, and material properties depending on the temperature are considered as well as the convection and radiation as boundary conditions. The stress distributions and distortion field are obtained. The welding residual stress and distortion are largely influenced by the welding sequences. When welding was performed continuously from one side to the other side, the magnitude of residual stress and distortion was the smallest.

Key words: T-joint; finite element simulation; welding sequence; residual stress; welding deformation

Influence of particle size on structure of HA/BG bioactive coatings ZHUANG Minghui, YIN Ke, LI Muqin, LI Xiaoxia (Provincial Key Laboratory of Biomaterials, Jiamusi University, Jiamusi 154007, China). p 41 - 44, 48

Abstract: HA/BG bioactive coatings were sprayed on Ti6Al4V substrate by subsonic flame spraying, and Ti/G coating was selected as transition player to relieve the stress in the coatings. HA/BG bioactive coatings underwent crystallization treatment at 700 ℃. The structure of the coatings was decided by the particle size. With fine particle, porous coatings can be obtained whose structure is beneficial to the bonding of the coatings and the bone tissue. After the crystallization treatment, the main phase of the HA/BG coatings was crystal HA, and the addition of fine active glass inhabited the growth of HA crystal. The compression stress exhibiting in HA/BG coatings was positive to improve the bonding strength of the coatings.

Key words: subsonic flame spraying; bioglass; transition player; particle size

AC arc stability of environmental protective type of basic and low hydrogen electrode MENG Gongge[1], CHU Jijun[2], LUAN Jingyue[2], GU Feng[1], LI Dan[1] (1. School of Material Science & Engineering, Harbin University of Science and Technology, Harbin 150040, China; 2. Harbin Welding Institute, China Academy of Machinery Science and Technology, Harbin 150080, China). p 45 - 48

Abstract: An electrode coating slag system CaO-CaF_2-BaO-TiO_2-SiO_2 has been designed base on analyzing several domestic and abroad basic slag systems. The experiments were done with uniform design method and computer aided analysis. Nine to eleven coating components were taken as independent variables and they were divided into five levels in all twenty nine experiments. The AC arc stability was taken as target function and data were analyzed with mathmatical statistic software. The results given the influencing trend figures of coating components on AC arc stability and multinomial mathematical model between independent variables and function. With these trend figures and mathematical model the improving direction of electrode for AC arc stability can be inquired and be searched target optimization.

Key words: basic electrode; AC arc stability; uniform design; optimization searching

TIG butt welding between Mg alloy and Al alloy filling with Zn wire LIU Fei, ZHANG Zhaodong, LIU Liming (Key Laboratory of Liaoning Advanced Welding and Joining Technology, School of Materials Science and Engineering, Dalian University of Technology, Dalian 116024, China). p 49 - 52

Abstract: Butt welding experiments of Mg to Al alloy filling with Zn wire were carried out by tungsten inert gas (TIG) welding. The welding joints were investigated and tested by metallography microscope, electronic probe micro-analyzer (EPMA), universal mechanical properties testing machine. The results indicated that the aluminum alloy 6061 and the magnesium alloy AZ31B was jointed with a good surface forming. The welded joints are mainly composed of $MgZn_2$, the zinc base solid solution and the aluminum base solid solution, there are not the obvious transitional layer between welded seam and aluminum base metal and the transitional layers which approximately 20 - 100 μm between welded seam and magnesium base metal. The hardness of the weld seam is higher than that of the base metal aluminium alloy 6061 and magnesium alloy AZ31B. The tensile strength of the butt joint is 75 MPa.

Key words: distributable metal of Mg and Al; butt welding filling with zinc wire; microstructures; mechanical properties; TIG

Strength and microstructure of Cu joints brazed with Cu-P based amorphous filler metal contained Zr GAO Fei, XU Weilong, WANG Chao, ZOU Jiasheng (Provincial Key Laboratory of Advanced Welding Technology, Jiangsu University of Science and Technology, Zhenjiang 212003, China). p 53 - 56

Abstract: The copper joints were brazed with CuP 7.7Sn5.4Ni14Si0.2Zr0.04 amorphous filler metal and conventional filler metal. The microstructures of filler metal and brazing joints were analyzed and the effect of brazing procedures on joints strength was studied. The results indicate that brazing procedures affect the strength of the brazing joints with both the CuP7.7Sn5.4Ni14Si0.2Zr0.04 amorphous filler metal and conventional filler metal. Compared to the amorphous brazing filler metal, conventional filler metal was more sensitive to the brazing procedure. In the same experimental conditions, shear strength of the joint brazed with amorphous brazing filler metal increased by 30% or more compared to the joint which brazed with conventional filler metal. CuP7.7Sn5.4Ni14Si0.2Zr0.04 amorphous brazing filler metal has no obvious phase structures in microscope, while the microstructure of conventional filler metal is mainly composed of primary $(Cu,Ni)_3P$ and $(\alpha$-$Cu + Cu_3P)$ eu-